JOURNAL OF APPLIED ELECTROCHEMISTRY 21 (1991) 55–59

Electrodeposition of Ni-transition alloys for the oxygen evolution reaction

HUI JUN MIAO, D. L. PIRON*

Département de Génie Métallurgique, Ecole Polytechnique de Montréal, C. P. 6079, succ. "A", Montréal, Québec H3C 3A7, Canada

Received 22 January 1990; revised 12 April 1990

The oxygen evolution reaction (OER) is the anodic reaction in several industrial electrolytic processes. The objective of this work was to develop a new electrocatalytic material for long-lasting and economical high performance electrodes. New electrodes were prepared by electrodeposition of nickel, nickel-ruthenium and nickel-iridium alloys. They were then activated by anodic polarization at 100 mA cm^{-2} to form an oxide layer. The electrocatalytic activity was characterized for the OER in 5 M KOH solution. The results show that nickel-iridium alloys provide greater electrocatalytic activity for the OER and better corrosion resistance than nickel-ruthenium in alkaline solution. The effects of transition elements on improving the performance of the nickel electrode are then discussed.

Notation

b	Tafel slope
i_{ex}	exchange current density
i_{dp}	electrodeposition current density
i_{OER}	oxygen evolution reaction current density
C_{dl}	double-layer capacity
η_{O_2}	oxygen overpotential

1. Introduction

The oxygen evolution reaction (OER) is an important reaction in the electrolysis of water, in electrosynthesis and in other processes where oxygen is anodically produced, such as in nickel, zinc and cobalt electrowinning.

The sulphate roast-leach-electrowinning process of zinc is very energy-intensive. The alkaline process, which differs from current practice in industry, has a lower specific energy consumption. St-Pierre and Piron have reported specific energy consumption of 1.75 kW kg^{-1} at 1000 A m^{-2} in alkaline solution [1] compared with 3.3 kWh kg^{-1} in classical industrial processes at 500 A m^{-2} [2]. Part of that high performance is obtained by using a stable oxide anode which catalyses the OER in alkaline solution and lowers the overpotential.

Nickel is frequently used to fabricate anodes for the OER [3–7]. However, the problem associated with long-term industrial applications is that the anode potential is not stable with time [6], which causes an increase in energy consumption. It is important to find a stable electrode that has a low overpotential in order to lower energy consumption in industrial applications. Improvements made by alloying nickel with elements such as lithium [7], iron [8, 9], chromium [10], titanium, iridium, ruthenium and tungsten [11], have been reported in the literature.

RuO_2 is a very good electrocatalyst for the OER, both in acid and in alkaline solutions [13–15]. However, Makaryvhev [16] and others [28] have shown that RuO_2/TiO_2 oxide suffers corrosion in KOH solution. This limits the use of pure ruthenium oxide as an electrocatalyst of the OER in a highly concentrated alkaline solution. Also, since the cost of this precious metal is still high, it is not economically attractive to use this kind of anode in electrowinning processes [17].

In alkaline solutions, IrO_2 showed a slightly higher Tafel slope (40–50 mV dec^{-1} [18, 19] compared with 30–50 mV dec^{-1} on RuO_2) and a higher overpotential than RuO_2 [20]. On the other hand, stabilization of RuO_2 by IrO_2 [21] and Ru-Ir alloys [22] has been reported in acid media during the anodic oxygen evolution reaction. This means that IrO_2 is electrochemically stable in acid media. In alkaline media, the iridium oxides are stable [23], but the performance and reaction mechanism of iridium oxide for the OER in alkaline media have not been well discussed.

In this investigation, the oxide electrocatalysts based on nickel and transition metals such as ruthenium and iridium were studied. Electrodes were prepared by electrolytic deposition of Ni, Ni-Ru and Ni-Ir alloys. The precious transition elements in nickel alloys are limited below to 10%. These alloys were anodically oxidized to obtain the mixed oxide surfaces, and these mixed oxide surfaces were then used to study the OER in KOH solution. By comparing the performance of the different electrodes, the respective beneficial effects of ruthenium and iridium elements were evaluated.

* To whom all correspondence should be sent.

0021-891X/90 $03.00 + .12

2. Experimental details

2.1. *Electrode preparation by electrodeposition*

Electrodeposition of nickel on 316 stainless steel gauze (48 mesh, Firth Brown Inox Ltd.) was conducted in a bath of $NiCl_2\ 6H_2O$ (240 g dm^{-3}, reagent grade) with the addition of $RuCl_3/IrCl_3$ (0.2–2.0 g dm^{-3}, reagent grade) at temperature of 55–75° C. The geometric surface area of the cathode was 1.0 × 1.0 cm^2. Two nickel plates (Ni, 99%) were used as anodes in the bath. To prepare the nickel electrode, the electrodeposition current density was between 35 and 350 mA cm^{-2} (based on geometric area). For the Ni-Ru and Ni-Ir alloys, the deposition current density was 200 mA cm^{-2}. The deposition amount was about 0.1 g cm^{-2} (geometric area). As the deposition current density changed, the deposition time was varied in order to maintain the same amount of deposit. The deposition bath was agitated by a magnetic stirrer. According to Moffatt [24], Ni-Ir alloys form continuous solid solutions in the full range of composition. For the Ni-Ru alloys, the solid solution exists up to about 20 wt % ruthenium [25]. The Ni-Ru alloys were examined by microscope and X-ray diffraction [26, 27]; the results show that solubility of ruthenium in nickel below 400° C was about 5 wt %. These results indicate that at least up to 5 wt % of ruthenium Ni-Ru alloy is the solid solution.

Before the electrochemical measurements were made, electrodes were activated by an anodic polarization at 100 mA cm^{-2} for over 30 min in 5 M KOH solution at room temperature. A stable oxidized surface was obtained which was verified by a reproducible polarization curve in the same testing conditions. Two oxide electrodes, RuO_2 and IrO_2, were prepared by the thermal decomposition method as described in [28].

2.2. *Morphological and chemical analyses*

Morphological and chemical analyses of anode surfaces were conducted using the scanning electron microscope (SEM) and energy dispersive spectrometer (EDS). The electrode chemical composition was given in wt %.

2.3. *Electrochemical measurements*

All measurements were made in 5 M KOH solution at room temperature (25 ± 3)° C. Two platinum plates (1.5 × 1.5 cm^2) were used as the counter electrodes. A saturated calomel electrode (SCE) was used as a reference electrode; it was inserted into the Luggin capillary which was mounted very close to the working electrode (< 2 mm).

The polarization curves and a.c. impedance were measured by using the Corrosion Measurement Software (Model 342) and the Electrochemical Impedance Software (Model 378) with the Potentiostat/Galvanostat (Model 273), provided by EG&G Princeton Applied Research Corp.. The current interruption technique available on the potentiostat was used to minimize the IR drop. The cyclic voltammograms were measured by the potentiostat/galvanostat and an IBM microcomputer.

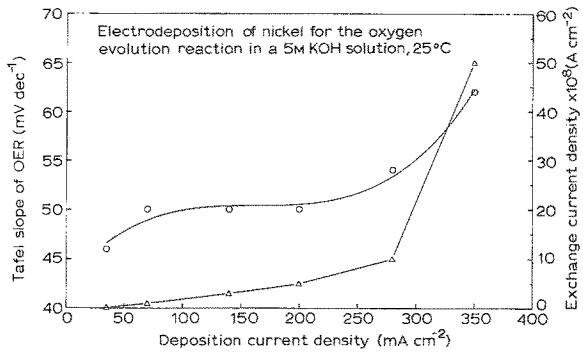

Fig. 1. Relationship between the Tafel slopes, b, and the exchange current densities, i_{ex}, of the OER on nickel anodes and the anode preparation current densities, i_{dp}. (○) Tafel slope, (△) exchange current density.

3. Results

Figure 1 shows the relationship between the Tafel slopes (b) and the exchange current densities (i_{ex}) of the OER on the nickel anodes and the anode preparation current densities (i_{dp}). The b was determined from the polarization curve by measuring the slope of the curve in the Tafel region. The polarization curves were obtained potentiodynamically. The scanning rate was 1 mV s^{-1} and the sweep direction was from less noble to noble potentials.

Figure 1 shows that the Tafel slopes (b) of the OER on the oxidized nickel electrodes are in the range of 50 mV dec^{-1}, at i_{dp} = 250 mA cm^{-2}. When i_{dp} is over 300 mA cm^{-2}, the b values increase rapidly and reach 62 mV dec^{-1} at i_{dp} = 350 mA cm^{-2}. However, the exchange current densities (i_{ex}) on the nickel electrodes increase as i_{dp} increases. The increase in the i_{ex} may result from the electrode surface roughness. As the surface roughness increases, the real surface area of the electrode increases and this results in an increase in i_{ex}. Figure 2 shows the double-layer capacitances (C_{dl}) of the oxidized nickel electrodes as a function of the deposition current densities (i_{dp}). The capacitance C_{dl}

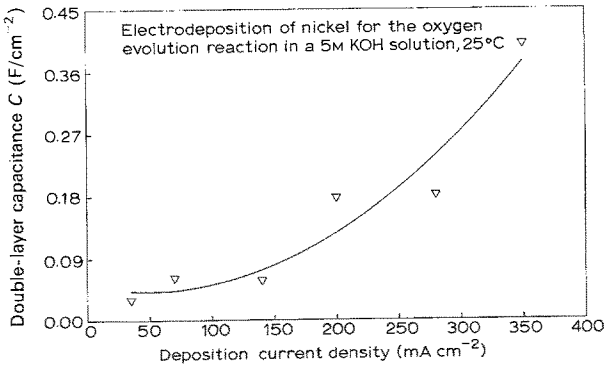

Fig. 2. The double-layer capacitances, C_{dl}, of the oxidized nickel electrodes as a function of the anode preparation current densities, i_{dp}. (▽) Capacitance measured at η = 300 mV.

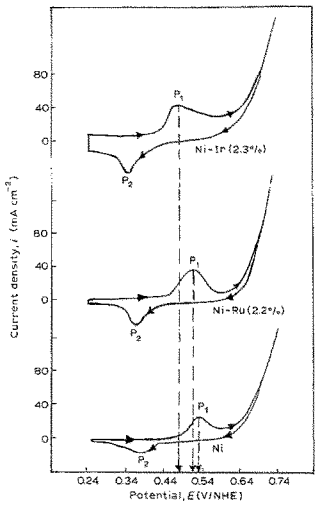

Fig. 3. The cyclic voltammograms of nickel, Ni-Ru and Ni-Ir alloys electrodes in 5 M KOH solution, at 25° C. Scanning rate: 20 mV s^{-1}.

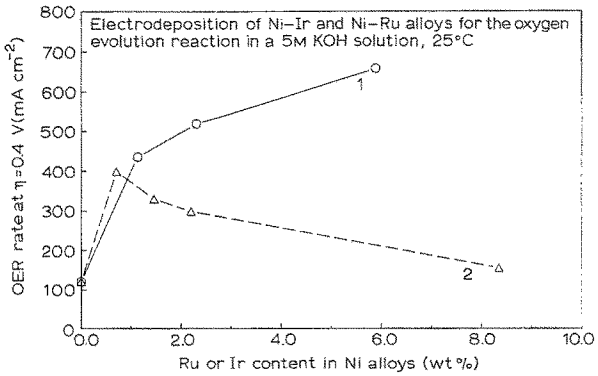

Fig. 4. The values of the OER current densities taken from the polarization curve at an overpotential of 0.4 V as a function of the ruthenium or iridium content in nickel alloy electrodes. Electrodeposition conditions: $NiCl_2$ $6H_2O$ 240 g dm^{-3} + Ir/Ru; i = 200 mA cm^{-2} for 30 min at 65° C. 1. (○) Ir_3, 2. (△) Ru.

was determined from the Nyquist plot. The a.c. impedance measurements were conducted at 300 mV overpotential of the OER. At this potential level, the Nyquist plot was easy to make. As we can see in Fig. 2, the C_{dl} increases with i_{dp}. This increase of C_{dl} could also correspond to an increase in the surface roughness and consequently in larger i_{ex} values (Fig. 1).

The cyclic voltammograms measured from electrodes of Ni, Ni-Ru and Ni-Ir are given in Fig. 3. The potential scanning rate was 20 mV sec^{-1}. All three curves show an oxidation peak (P_1) before the OER on the initial anodic direction. These peak potentials were shifted to less noble values by adding ruthenium and iridium to the nickel electrodes. The peak potential of the Ni-Ir alloy appered 56 mV before that of nickel, while the difference between peak potentials of Ni and Ni-Ru electrodes was only 10 mV. In the return direction, the peaks (P_2) were also observed at more active potentials than that of P_1. P_2 peaks on all three curves had nearly the same potential values. The OER overpotential (η_{O_2}) measured at 20 mA cm^{-2} was lowered by the presence of the ruthenium and iridium by 30 and 40 mV, respectively. Table 1 summarizes the data obtained from the cyclic voltammograms.

Figure 4 gives the value of the OER current density taken from the polarization curve at an overpotential of 0.4 V as a function of the ruthenium or iridium content in the nickel alloy electrodes. As can be seen for both Ni-Ru and Ni-Ir electrodes, the beneficial effects obtained by the presence of the additional elements are more significant for the first 1% of the transition elements. With further additions, Ir increases the i_{OER} to a small extent; in the case of ruthenium, an adverse effect is observed. Measurement of the OER current density at 0.4 V overpotential shows that 6 wt % of iridium increases the i_{OER} 6 times, while the best results for the Ni-Ru electrode is obtained at 1 wt % of ruthenium, for an increase of 4 times compared with the value of i_{OER} on the nickel electrode.

Pure RuO_2 and IrO_2 oxide electrodes were prepared and tested for comparison with the nickel oxide data. Table 2 shows the value of the thermodynamically calculated and measured oxidation peak potentials for the Ni oxide, RuO_2 and IrO_2 electrodes in 5 M KOH solution at 25° C. The thermodynamic potentials of oxidation for Ni^{3+}/Ni^{4+}, Ru^{4+}/R^{8+} and Ir^{4+}/Ir^{6+} were calculated [23] and compared with measured oxidation peak potentials observed in the cyclic voltammograms. The pH value was 14.93, as calculated using the mean activity coefficients from reference [29]. Table 2 gives the results. It shows that the maximal difference between these two values is within 15 mV; they correspond very well. The highest measured peak potential is 0.534 V on nickel oxide, while ruthenium and iridium oxides show peak potentials of 0.490 V (Ru^{4+}/Ru^{8+}) and 0.300 V (Ir^{4+}/Ir^{6+}) respectively.

Table 1. Summary of the data from cyclic voltammograms of Fig. 3.

Deposit content (wt %)	P_1 *(V NHE)*	*Shift (mV)*	η_{O_2} *(mV)*	$\eta_{O_{2dec}}$ *(mV)*
Ni99.7	0.534	–	310	–
Ni97.8, Ru2.2	0.524	10	280	30
Ni96.6, Ir2.3	0.478	56	270	40

P_1 redox peak potential

η_{O_2} oxygen overpotential at 20 mA cm^{-2}.

$\eta_{O_{2dec}}$ decrease in O_2 overpotential as compared with nickel electrode.

Table 2. Thermodynamic and measured oxidation potential values

Electrode	*Oxides*	E_c (*NHE*)	E_{p_1} (*NHE*)
Ni oxide	Ni^{3+}/Ni^{4+}	0.538	0.534
Ru oxide	Ru^{4+}/Ru^{8+}	0.505	0.490
Ir oxide	Ir^{4+}/Ir^{6+}	0.290	0.300

E_c are thermodynamically calculated potentials [23], pH = 14.93, 25° C.
E_{p_1} is the oxidation peak potentials measured in 5 M KOH solution, 25° C.

4. Discussion

4.1. *The overall oxygen overpotential*

The presence of ruthenium and iridium in the nickel electrode decreased the OER overpotential by 30 and 40 mV respectively (Table 1). This indicates an even better effect for iridium than ruthenium on the electrocatalytic properties of the mixed surface oxide electrode with respect to the OER in KOH solution in this test. The performance of the electrode for the OER has been attributed to the surface concentration of the active site on the oxide layer [28]. The presence of small amounts of ruthenium or iridium species in the oxide layer would favour the formation of such special sites and increase the catalytic effect even the surface oxide is still dominated by the nickel oxide. Such an explanation was previously provided to explain the beneficial effects of ruthenium oxide in acid media [21].

As observed in the cyclic voltammograms of Fig. 3, the forward potential sweep showed a potential peak (P_1) before the OER. The overpotential for oxygen evolution may be divided into two parts (see Fig. 5), according to the following equation:

$$\eta_{O_2} = \Delta E_{ox} + \Delta E_{O_2}$$

where ΔE_{ox} is considered to be a polarization between the reversible oxygen potential and the electrode surface oxidation potential (P_1); ΔE_{O_2} as the potential difference between the OER (e.g. $i = 20\,mA\,cm^{-2}$) and the peak (P_1) potential.

Table 3 shows the separated overpotential values in terms of ΔE_{ox} and ΔE_{O_2}. The lowest ΔE_{O_2} value belongs to the Ni-Ru oxide electrode and the highest ΔE_{O_2} value appears on the Ni-Ir oxide electrode. The nickel oxide is in the middle. In the case of ΔE_{ox}, the position is different. The lowest ΔE_{ox} value corresponds to the Ni-Ir oxide electrode and the highest to the nickel oxide electrode.

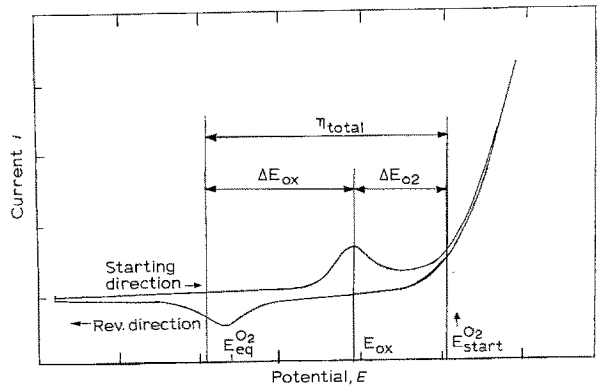

Fig. 5. Illustration dividing the overall overpotential η_{O_2} into two parts, $\Delta E_{ox} + \Delta E_{O_2}$.

Table 3. Oxygen evolution overpotential ($i_{OER} = 20\,mA\,cm^{-2}$) on the tested electrode

Electrode	ΔE_{ox} (*mV*)	ΔE_{O_2} (*mV*)	η_{O_2} (*mV*)
Ni	188	122	310
Ni-Ru	178	102	280
Ni-Ir	132	138	270

4.2. *The peak potential*

The oxidation potential peaks were observed both on the pure metal oxide and on the mixed oxide electrodes. In the case of the pure metal oxide, the peak potential was observed at a value very close to the thermodynamic potential calculated for the oxide Ni^{3+}/Ni^{4+}, Ru^{4+}/Ru^{8+} and Ir^{4+}/Ir^{6+}. It can be seen that the peak potential for ruthenium oxide is rather close to that on the nickel oxide; it appears only 44 mV before the nickel oxide peak (Table 2, E_{P_1}). The iridium oxide peak is observed at a much less nobel value and appears at some 234 mV before the nickel oxide peak.

Although the nickel surface oxide dominant the surface oxidation reaction, the presence of iridium in the nickel oxide results in displacement of the Ni^{3+}/Ni^{4+} peak position to a lower value, which decreases the ΔE_{ox} value on Ni-Ir electrode (Table 3). Since the OER takes place on the higher oxide formed at the peak potential, it is possible to say that the catalytic oxide layer formed by oxidation of Ni^{3+}/Ni^{4+} is easier on Ni-Ir oxide than on Ni-Ru oxide.

4.3. ΔE_{O_2}.

The second part of the η_{O_2}, ΔE_{O_2}, represents the effectiveness of the electrocatalytic power of the mixed oxide surface, because the OER always takes place on an oxidized surface.

Table 3 shows that the Ni-Ru oxide has the lowest ΔE_{O_2} value and corresponds to a better and more effective electrocatalytic mixed oxide surface for the OER.

The larger value of the ΔE_{O_2} for the Ni-Ir oxide (Table 3) indicates that this mixed oxide layer may be less electrocatalytically active. However, the total overpotential of the Ni-Ir oxide remained at about the same level as that of the Ni-Ru oxides. This is because of the lower value of ΔE_{ox} in the case of the Ni-Ir oxide. The lower value of ΔE_{ox} compensated for the higher value of the ΔE_{O_2} when the total overpotential is counted.

4.4. *Corrosion behaviour*

Although the overall overpotential η_{O_2} is rather similar for both mixed oxides, their stability in alkaline solution is not the same. Corrosion of the ruthenium oxide on the surface layer produces a loss of electrocatalytic properties. The higher the ruthenium content, the more rapidly the electrode corrodes [16]. This was also observed in our test conditions. The uncoloured solution turned to yellow after 30 min polarization of the Ni-Ru electrode at a 100 mA cm^{-2} current density. The surface chemical analysis showed almost no ruthenium on the tested electrode surface. This is why the Ni-Ru oxide containing 2% or more ruthenium showed almost the same catalytic effect as the pure nickel oxide after immersing the electrode in 5 M KOH solution for more than 30 min.

By comparison, the Ni-Ir mixed oxide electrode in this investigation was much more stable and retained its good electrocatalytic activity for more than 24 h at 100 mA cm^{-2} current density in our test.

5. Conclusions

Ruthenium and iridium in the mixed oxide layer of nickel electrodes both significantly lower the oxygen evolution reaction overpotential.

Ruthenium tends to corrode out of the mixed oxide electrode, which then loses some of its electrocatalytic properties for the OER.

The Ni-Ir oxide resists corrosion well and retains its good electrocatalytic property for at least 24 h in our long-term test.

In anodic potential sweep experiments, the peak potentials were observed before the OER. This peak was attributed to the formation of an oxide at a higher level of oxidation.

The OER overpotential may be divided into two parts: $\eta_{O_2} = \Delta E_{ox} + \Delta E_{O_2}$. ΔE_{ox} which characterized the peak potential was the lowest in the case of the Ni-Ir mixed oxide; ΔE_{O_2} which presented the potential difference between the peak and the OER was the lowest in the case of the Ni-Ru mixed oxide.

References

[1] J. St-Pierre and D. L. Piron, *J. Appl. Electrochem.* **16** (1986) 447.
[2] A. P. Brown, J. H. Melsenhelder and N. P. Yao, *Ind. Eng. Chem. Prod. Res. Dev.* **22**(1983) 263.
[3] J. P. Hoare, 'The Electrochemistry of Oxygen', Interscience, New York (1968).
[4] J. O'M Bockris and S. Srinivasan, 'Fuel Cells, Their Electrochemistry', McGraw-Hill Book Co., New York (1969) ch. 8.
[5] M. H. Mill, G. Kissel, P. W. Lu and S. Srinivasan, *J. Electrochem. Soc.* **123** (1976) 332.
[6] P. W. T. Lu and S. Srinivasan, *J. Electrochem. Soc.* **125** (1978) 265.
[7] J. C. Batejue Nadesan and A. C. C. Tseung, *J. Electrochem. Soc.* **132** (1985) 2957.
[8] M. de K. Thompson and A. L. Kaye, *Trans. Electrochem. Soc.* **60** (1931) 229.
[9] G. Grube and W. Gaupp, *Z. Elektrochem.* **45** (1939) 290.
[10] M. de K. Thompson and G. H. Sistare Jr., *Trans. Electrochem. Soc.* **78** (1940) 259.
[11] D. A. Thompson, J. A. Davies and W. W. Smeltzer, Ion Implant. Met., 3rd Int. Conf. Modef. Surf. Prop. Met. Ion Implant (1981).
[12] US Patent 4 363 706.
[13] E. Yeager, National Bureau of Standards. USA Special Pub. 455 (1976) 203.
[14] G. Singh, M. H. Miles and S. Srinivasan, [13] p. 289.
[15] A. C. C. Tseung and S. Jasem, *Electrochim. Acta* **22** (1971) 31.
[16] Yu. B. Makarychev, E. K. Spasskaya, S. D. Khodkevich and L. M. Yakimenko, *Electrokhimiya* **12** (1976) 994.
[17] V. A. Ettle, *CIM Bull.* **70** (1977) 179.
[18] C. Iwakura, H. Tada and H. Tamura, *Denki Kagaku* **45** (1977) 202.
[19] H. Miles, Y. H. Huang and S. Srinivasan, *J. Electrochem. Soc.* **125** (1978) 131.
[20] Electrodes of Conductive Metallic Oxide, Part B, (edited by Sergio Trasatti), Elsevier Science, New York (1981).
[21] R. Kötz and S. Stucki, *Electrochim Acta* **31** (1986) 1311.
[22] *Idem, J. Electrochem. Soc.* **132** (1985) 103.
[23] M. Pourbaix, 'Atlas of Electrochemical Equilibria in Aqueous Solution', NACE, Houston, USA (1974).
[24] W. G. Moffatt, 'The Handbook of Binary Phase', Genium Publications, (1988).
[25] C. Manders, *Ann. Phys.* **5** (1936) 181.
[26] E. Raub and D. Menzel, *Z. Metallkd.* **52** (1961) 831.
[27] I. I. Kornilov and K. P. Myasnikova, *TR: Russ. Met. Min.* **4** (1964) 95.
[28] S. Trasatti and W. E. O'Grady, 'Advances in Electrochemistry and Electrochemical Engineering', Vol. 12, John Wiley & Sons, New York (1981) 177.
[29] D. Dobos, 'Electrochemical Data', Elsevier Science, New York (1975) 207.